Journal of Biomaterials Science, Polymer Edition
Publication details, including instructions for authors and subscription information:
http://www.tandfonline.com/loi/tbsp20

Improved bioactivity of PAN-based carbon nanofibers decorated with bioglass nanoparticles

Bing Han[a], Xuehui Zhang[bd], Haiyang Liu[cd], Xuliang Deng[b], Qing Cai[c], Xiaolong Jia[c], Xiaoping Yang[c], Yan Wei[b] & Gang Li[c]

[a] Department of Orthodontics, School and Hospital of Stomatology, Peking University, Beijing 100081, P.R. China

[b] Key Laboratory of Carbon Fiber and Functional Polymers, Ministry of Education, Beijing University of Chemical Technology, Beijing 100029, P.R. China

[c] State Key Laboratory of New Ceramics and Fine Processing, Department of Materials Science and Engineering, Tsinghua University, Beijing 100084, P.R. China

[d] Department of Geriatric Dentistry, School and Hospital of Stomatology, Peking University, Beijing 100081, P.R. China

Published online: 22 Nov 2013.

To cite this article: Bing Han, Xuehui Zhang, Haiyang Liu, Xuliang Deng, Qing Cai, Xiaolong Jia, Xiaoping Yang, Yan Wei & Gang Li , Journal of Biomaterials Science, Polymer Edition (2013): Improved bioactivity of PAN-based carbon nanofibers decorated with bioglass nanoparticles, Journal of Biomaterials Science, Polymer Edition, DOI: 10.1080/09205063.2013.861169

To link to this article: http://dx.doi.org/10.1080/09205063.2013.861169

Journal of Biomaterials Science, Polymer Edition, 2013
http://dx.doi.org/10.1080/09205063.2013.861169

Taylor & Francis
Taylor & Francis Group

Improved bioactivity of PAN-based carbon nanofibers decorated with bioglass nanoparticles

Bing Han[a#], Xuehui Zhang[b,d#], Haiyang Liu[c,d], Xuliang Deng[b], Qing Cai[c], Xiaolong Jia[c], Xiaoping Yang[c], Yan Wei[b]* and Gang Li[c]*

[a]*Department of Orthodontics, School and Hospital of Stomatology, Peking University, Beijing 100081, P.R. China;* [b]*Key Laboratory of Carbon Fiber and Functional Polymers, Ministry of Education, Beijing University of Chemical Technology, Beijing 100029, P.R. China;* [c]*State Key Laboratory of New Ceramics and Fine Processing, Department of Materials Science and Engineering, Tsinghua University, Beijing 100084, P.R. China;* [d]*Department of Geriatric Dentistry, School and Hospital of Stomatology, Peking University, Beijing 100081, P.R. China*

(*Received 24 August 2013; accepted 25 October 2013*)

Composite nanofibers composed of polyacrylonitrile (PAN)-based carbon nanofibers and bioactive glass (BG) nanoparticles have been prepared by electrospinning and *in situ* sintering. Morphology observation showed that the BG nanoparticles of size 20–50 nm were uniformly distributed on the surface of composite nanofibers with 350 nm average diameter after carbonization. Biological mineralization indicated the formation of apatite-like layer on the surface of composite nanofibers, in which the composition of carbonate hydroxyapatite was proved by FTIR and XRD analysis. Cell growth dynamics according to cellular morphology, CCK-8 assay, and alkaline phosphatase activity assay exhibited better cell adhesion, proliferation, and osteogenic induction of bone marrow-derived mesenchymal stem cells cultured on the composite nanofibers, which suggested the higher bioactivity of composite nanofibers compared to pure PAN-based carbon nanofibers.

Keywords: carbon nanofiber; bioglass; eletrospinning

Introduction

Polyacrylonitrile (PAN)-based carbon fibers (CFs) have long been considered for the application of tissue engineering due to exceptional mechanical properties, such as flexural and fatigue strength, high strength-to-weight ratio, etc.[1–3] Compared to the commercial CFs, PAN-based carbon nanofibers (CNFs) were more favorable to fabricate biomedical materials for their intrinsic advantages such as larger surface, higher aspect ratio, and more prominent surface effect.[4–7] Furthermore, the smaller-scale CNFs (diameter 100 nm or less) have been considered to promote the adhesion of osteoblasts and simultaneously impair the adhesion of fibroblast,[6] which was regarded as potential biomaterials in bone regeneration. However, as bio-inert materials, CNFs did not contain functional groups that could attract calcium cations and phosphate anions to initiate the crystallization of carbonate hydroxyapatite (CHA).[8–10] Therefore, it was highly desirable to decorate CNFs with bioactive materials to expand and optimize the application of CNFs in bio-technological fields.

*Corresponding authors. Email: kqdxl@bjmu.edu.cn (Y. Wei); ligang@mail.buct.edu.cn (G. Li)
#These authors contributed equally to this work.

Bioactive glass (BG) with excellent bioactivity and osteointegration ability has been widely used in orthopaedic applications. A certain composition of silicate glass has been reported to chemically bond with living bone, and the mechanism of which was attributed to the formation of an apatite layer on its surface.[11–13] BG also showed excellent bioactive behavior in physiological fluids to release ions favoring apatite formation.[14] Meanwhile, BG has been demonstrated to be capable of creating a bond with soft tissue.[15] Taken together, BG may be a promising bioactive modifier to improve the intrinsic physiological drawback of CNFs.

Therefore, the BG particles were controlled doping on the surface of PAN-based carbon nanofibers in a similar way as two types of β-TCP/CNFs, we previously made.[16,17] The BG/CNF composite nanofibers were fabricated by electrospinning PAN-based solution and followed by *in situ* sintering. The time-dependent biomineralization behaviors of BG/CNF composite nanofibers in simulated body fluid (5SBF) were evaluated. The biocompatibility of BG/CNF composite nanofibers was investigated by the cell growth dynamics of bone marrow-derived mesenchymal stem cells (BMSCs) seeded on composite nanofibrous membranes.

Materials and methods

Materials

PAN (Mw = 100,000 g/mol, 93.0 wt.% acrylonitrile, 5.3 wt.% methylacrylate, and 1.7 wt.% itaconic acid) was produced by Courtaulds Co. UK. Triethyl phosphate (TEP), calcium nitrate tetrahydrate (CN), tetraethoxysilane (TEOS), Ethylene Diamine Tetraacetic Acid (EDTA), and trypsin were supplied by Aldrich Trading Co. Ltd. N,N′-Dimethylformamide (DMF, analytic pure, P99.5%) and other chemical agents were purchased from Beijing Fine Chemical Co. Rat BMSCs, Penicillin-Streptomycin, and Glutamine were obtained from Cyagen Biosciences Inc. (Guangzhou, China). The Dulbecco's modified Eagle's medium, fetal bovine serum (FBS), trypsinase, and Alkaline Phosphatase (ALP) Assay Kit were purchased from Sigma Trading Co. Ltd (St. Louis, MO, USA).

Fabrication of BG/CNF composite nanofibers

The illustration of the experiment process is shown in Figure 1. Firstly, 3 mL TEP was dissolved in 1 mL distilled water and stirred thoroughly at 353 K for 48 h to obtain a hydrolyzed TEP solution. Then, 0.476 mL of the prepared solution, 0.462 g CN, and 0.865 mL TEOS (The BG of composition in mole % of 58% SiO_2–33% CaO–9% P_2O_5 [18]) were added in turn into 20 mL N,N′-DMF containing 10 wt.% PAN, and stirred at room temperature for 6 h to obtain a homogeneous solution.

For electrospinning, 10 mL of the solution was fed into a 20 mL syringe and injected through a needle (diameter 0.5 mm) at an injection rate of 0.3 mL h^{-1} using a syringe pump (TOP 5300), and an applied voltage (DW-P303-1AC, China) was kept at 1 kV cm^{-1} to a mandrel, which was rotated at a speed of 12 ms^{-1}.

The electrospun PAN-based nanofibers were stabilized at 553 K for 30 min in air, and subsequently carbonized at 1273 K for 2 h with a heating rate of 5 K min^{-1} in highly pure N_2 to obtain the composite nanofibers and the pure CNFs.

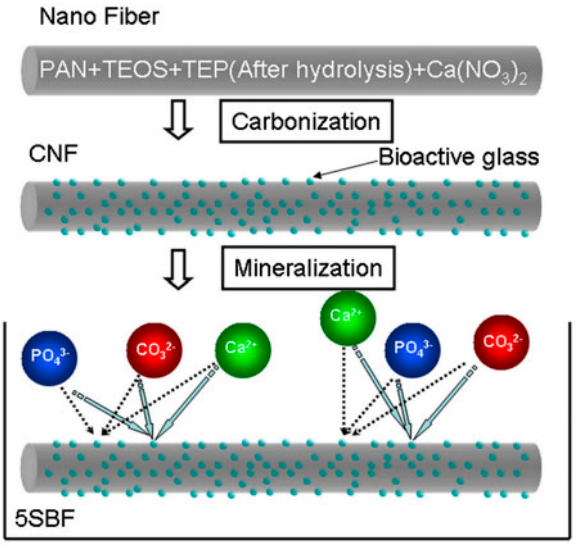

Figure 1. Schematic illustration for the preparation of BG/CNF composite nanofibers and its mineralization.

Characterizations

The surface morphologies of nanofibers and cellular morphology were observed by field emission scanning electron microscope (FE-SEM, Hitachi S-4700) at 20 kV using Pt coated samples. The elements analysis was performed under energy disperse X-ray spectroscopy (EDS, EDAXGENESIS2000). The chemical interaction was analyzed using the diffuse reflectance Fourier transform infra-red spectroscopy (FTIR Magna 750R, Nicolet, USA). X-ray diffraction patterns were collected using a X-ray diffractometer (XRD, Rigaku D/max 2500 VB2+/PC) operating at 40 kV and 200 mA.

Biological mineralization

In order to assess the bioactivity of the composite nanofibers, the *in vitro* mineralization was carried out in five times concentrated simulated body fluid (5SBF), which accelerated the classical biomimetic process from 7–14 days to 1 day, as shown in the schematic illustration of Figure 1. The 5SBF was prepared by following Barrere's method with the ion concentrations as below: NaCl (733.5 mM), $MgCl_2{\cdot}6H_2O$ (7.5 mM), $CaCl_2{\cdot}2H_2O$ (12.5 mM), Na_2HPO_4 (5.0 mM), and $NaHCO_3$ (21.0 mM). The solution was kept at 37 °C, and the pH was regulated to be between 6.3 and 6.5.[19] The composite nanofibers were soaked in SBF solution for 6, 18, and 30 h, respectively, and were removed and washed with ethanol. The composite nanofibers without soaking in SBF solution were choosed as the control.

Cell growth dynamics

Cell culture and seeding

The culture medium contained Rat Mesenchymal Stem Cell Basal Medium supplemented with 10% Mesenchymal Stem Cell-Qualified FBS, 100 IU/mL Penicillin-Streptomycin,

and 2 mM Glutamine. Once BMSCs reached 80–90% confluence, cells were detached with 0.25% trypsin/EDTA and subcultured at a density of 5×10^5 cells in a T75 flask. BMSCs were passaged three times before being used. BG/CNF nanofibrous membranes were placed into 6-well plates and sterilized with ultraviolet light for 1 h. Cells were cultured on these membranes in medium with osteogenic additives, including 50 mg/mL ascorbic acid, 10 mM sodium b-glycerol phosphate, and 10^{-8} M dexamethasone. Control cells were cultured on TCPs without any osteogenic additives. All experiments were done in triplicate.

Cellular morphology observation

The cellular morphology was observed after cells were cultured on nanofibrous membranes for 1, 3, and 5 days. BMSCs were washed with PBS and fixed with 2.5% glutaraldehyde for 2 h, and then treated with 0.18 M sucrose solution. The samples were rinsed three times with water, and then dehydrated through a series of graded alcohol solutions before being air-dried overnight. The scaffolds were coated with gold using a sputter coater before observation.

Cell proliferation analysis

Cell proliferation was evaluated using a Cell Counting Kit based on WST-8. After cells were cultured on nanofibrous membranes for 4 h, 1, 3, and 5 days, the WST-8 reagent was added, and incubated for another 4 h protected from light. Then, 200 μL of each sample was added to a 96-well plate, and the absorbance was measured at 450 nm using a microplate reader (Bio-Rad 680, Microplate Master, Hercules, CA, USA).

ALP activity assay

ALP activity of BMSCs cultured for 3, 7, and 14 days was measured using the ALP Assay Kit according to the manufacturer's instructions. The kit uses p-nitrophenyl phosphate (pNPP) as a phosphatase substrate which turns yellow when dephosphorylated by ALP. From each well 30 μL culture supernatants were collected. Samples were put in alkaline buffer, and added with 50 μL pNPP solution. After incubation for 60 min, the reaction was stopped with 20 μL stop solution. Then the absorbance was measured with 405 nm. This experiment was based on standard curve which from Kit itself to quantify ALP activity.

The above experimental results and measurements were performed in triplicate and expressed as the mean ± standard deviation. Statistical analysis was performed using the Student's paired *t*-test, and *p* values less than 0.05 were considered significant.

Results and discussion

Mechanism schematic of BG/CNF composite nanofiber preparation

For PAN-based CNFs doped with different contents, different morphologies in the sintering process were observed, which was attributed to the dopant particle migration and aggregation,[16,17] as shown in the mechanism schematic of Figure 2. As seen from Figure 2(a), *in situ* phase separation occurs between the matrix and dopant as the temperature increased. In the meantime, many small dopant particles were formed in matrix which had a large surface free energy. However, these particles were thermodynamically

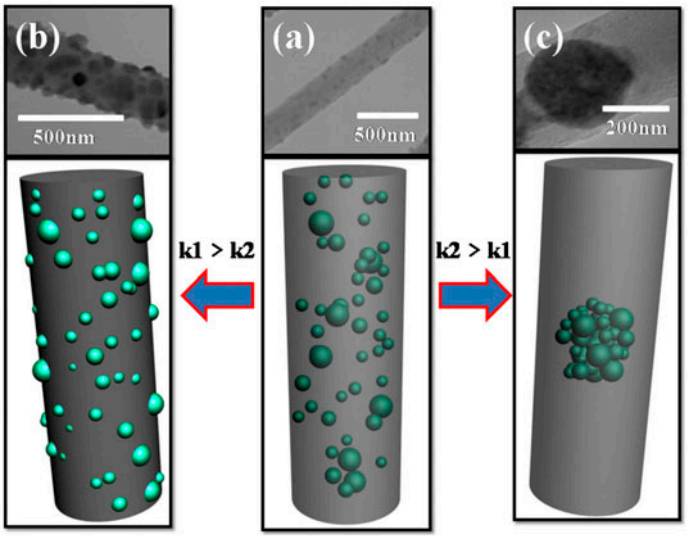

Figure 2. Mechanism schematic for particle migration and aggregation in sintering process, TEM images for different stage ((a) composite nanofiber after *in situ* phase separation, (b) composite nanofiber after migration, and (c) composite nanofiber after aggregation) are set on the top of the diagram.

unstable, which led them migrate to the surface of the matrix and aggregate in the matrix for reducing the energy. The model used for the sintering process was based on the Gibbs-Thompson relation, and intrinsic to this formula were two constants: the surface free energy and the particle volume.[20] According to this formula, we defined the rate constant of particle migration as $k1$, corresponding aggregation rate constant as $k2$. As seen in Figure 2(b), the space between particles was large when doped with low content, and the particle migration is dominant ($k1 > k2$). As a contrary, when the matrix was doped with high content, the aggregation was dominant ($k2 > k1$), shown in Figure 2(c).

Morphology of BG/CNF composite nanofibers

Figure 3 shows the SEM images of the as-spun PAN-based nanofibers and nanofibers after carbonization. As seen from Figure 3(a), the PAN-based nanofibers exhibited a millimeter-length-scale fibrous morphology with an average diameter ~450 nm, which showed a partial alignment along the rolling direction. After stabilization at 533 K in air and carbonization at 1273 K in nitrogen, small BG nanoparticles with 20–50 nm size were decorated and distributed uniformly on the surface of PAN-based CNFs, as shown in Figure 3(b). Furthermore, the average diameter of the nanofibers decreased to 350 nm, due to the cyclization, decyanation, and denitrogenation during the carbonization, which resulted in the loss of the methylacrylate comonomer and other substitutional groups from the nanofibers.[21,22]

Biological mineralization

Morphology development of BG/CNF composite nanofiber mineralization

In order to investigate the degradation and bioactivity of BG/CNF composite nanofibers *in vitro* physiological environment, the morphology development and constituent

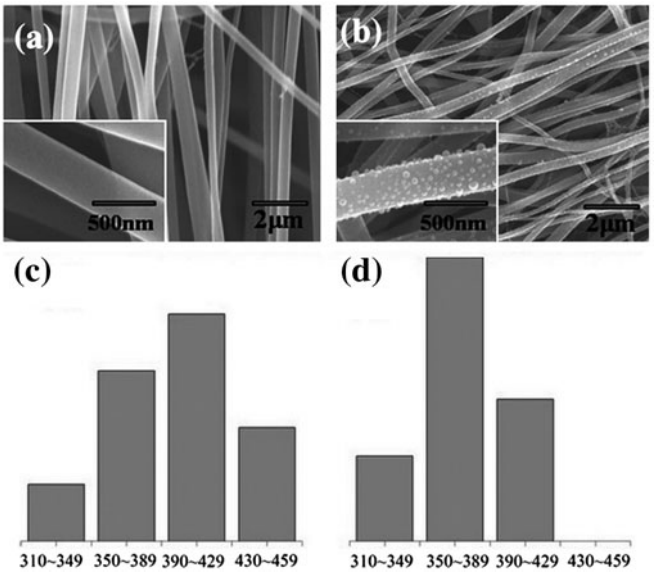

Figure 3. SEM images and fiber diameter distribution of the as-spun PAN-based nanofibers (a, c) and nanofibers after carbonization (b, d). Inserts show the magnifications of the nanofibers.

structure of composite nanofibers were characterized and analyzed. The morphology development of BG/CNF composite nanofibers and PAN nanofibers after different soaking times in 5SBF is shown in Figure 4. For PAN-based nanofibers, the surface of the nanofibers was flat and smooth before and after soaking, as shown in Figure 4(a) and (b). However, the surface of BG/CNF composite nanofibers was covered by a number of spherical particles less than 80 nm in diameter after 6 h of immersion, shown in Figure 4(d). With the extension of soaking time, the size of spherical particles grew larger and almost covered the whole surface of BG/CNF composite nanofibers, shown

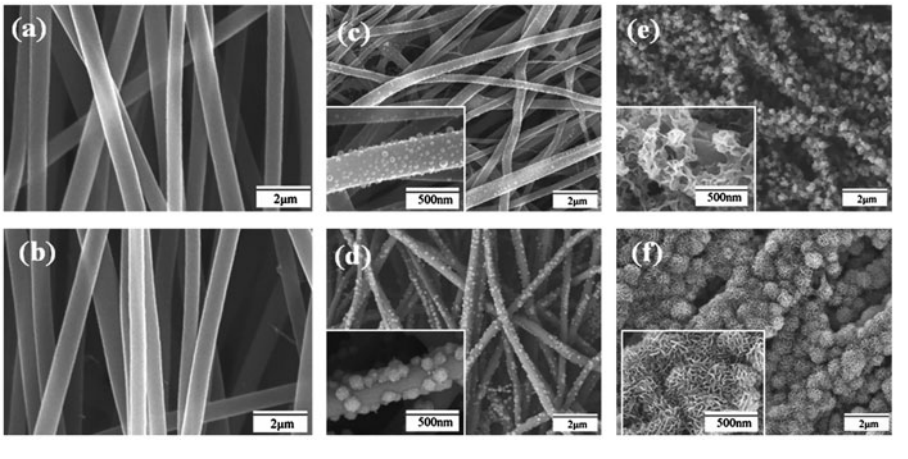

Figure 4. SEM images of PAN nanofibers before (a) and after soaking in 5SBF for 30 h (b), BG/CNF composite nanofibers before (c) and after soaking in 5SBF for (d) 6, (e) 18, (f) 30 h. Insets show the magnifications of the nanofibers.

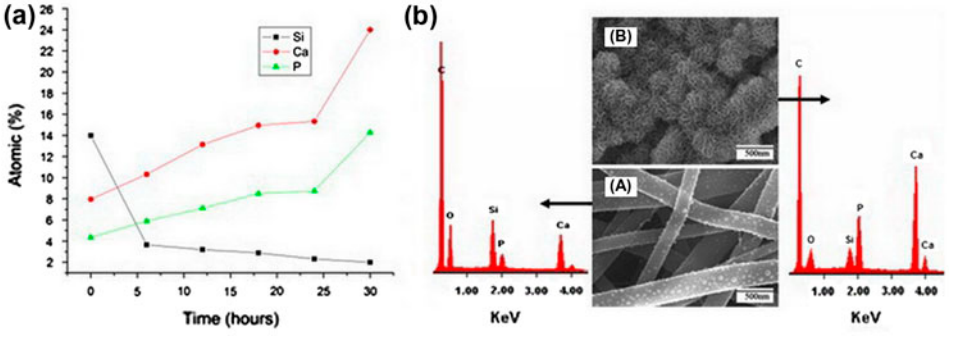

Figure 5. (a) EDS patterns obtained at different time and (b) SEM images and element analysis results after soaking in 5SBF for (A) 0 h and (B) 30 h.

in Figure 4(e). However, after soaking in 5SBF for 30 h, an obvious change in both size and morphology of spherical particles was observed in Figure 4(f) due to the increased mineralization rate. In fact, the spherical particles with average diameter ~700 nm were constituted of hundreds of acicular crystals, which suggested that the apatite-like layer was formed on the surface of the BG/CNF composite nanofibers.

Figure 5 shows energy dispersive spectroscopy (EDS) patterns of BG/CNF composite nanofibers obtained at different time and element analysis results before and after soaking in 5SBF. The obtained element analysis of the BG/CNF composite nanofibers without soaking in the 5SBF agreed well with the nominal glass composition, that is 58% SiO_2-33% CaO-9% P_2O_5 (in mole %). With increasing the soaking time, the EDS pattern exhibited a gradual increase in the Ca and P signal and a corresponding attenuation of the Si signals, and the sharp increase of Ca and P signal after 30 h of soaking indicated the formation of an apatite-like material, which was consistent with the SEM results. The Ca/P molar ratio exhibited gradual decreasing tendency, and the value obtained by EDS was 1.68 for 30 h of incubation, which was very similar to the Ca/P molar ratio characteristic of stoichiometric HA (1.67).[23]

FTTR analysis

Figure 6 shows the FTIR spectra of BG/CNF composite nanofibers after soaking in 5SBF for different time. The peaks at 1242 and 460 cm^{-1} in the spectra of BG/CNF composite nanofibers without soaking were corresponded to P=O double band and Si–O–Si band, respectively. After 6 h soaking in 5SBF solution, the obvious peak at 1037 cm^{-1} was attributed to P–O stretching vibration, and the peaks at 879 and 564 cm^{-1} were resulted from CO and P–O bending vibration. After 30 h soaking in 5SBF solution, the broad and one-component bands at 1037 and 564 cm^{-1} corresponded to phosphate groups (PO_4^{3-}), while the band located at 868 cm^{-1} corresponded to HPO_4^{2-} groups, which were the disordered characteristic of featureless PO_4^{3-} bands.[18] The three bands at 1462, 1410 and 879 cm^{-1} were assigned as to CO_3^{2-} groups, which implied that the poorly crystallized or amorphous carbonated Ca–P phase was precipitated on the surface of nanofibers. With the prolong of soaking time in the 5SBF solution, an increase in the intensity of the phosphate and carbonate peaks can be observed, which was similar to those observed in synthetic CHA.[24] FTIR analysis indicated the formation of CHA on the surface of BG/CNF composite nanofibers after biological mineralization.

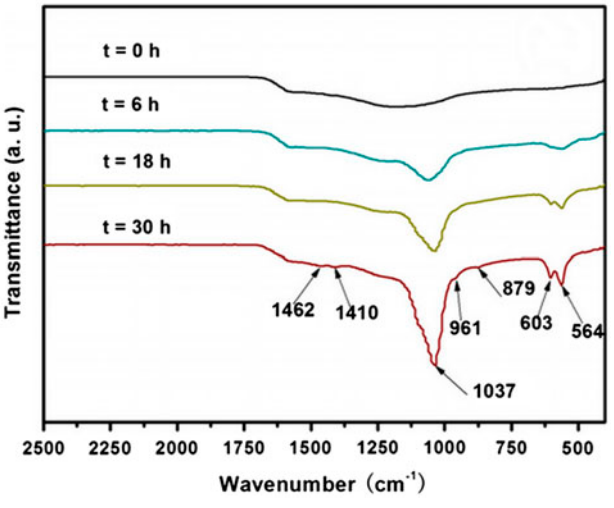

Figure 6. FTIR spectra of BG/CNF composite nanofibers after soaking in 5SBF for different time.

XRD analysis

Figure 7 shows the XRD patterns of BG/CNF composite nanofibers after soaking in 5SBF for different time. After soaking in 5SBF for 6 h, two weak diffraction peaks of an apatite-like phase at $2\theta = 32^{o}$ and 37^{o} appeared, which corresponded to the (2 1 1) and (1 3 0) crystal planes of apatite. After soaking in 5SBF for 18 h, an obvious peak at $2\theta = 25^{o}$ assigned to (0 0 2) crystal plane of apatite was observed. With extending the soaking time, the characteristic peaks of apatite became stronger, which implied that the crystal degree and amount of CHA increased. However, after soaking in 5SBF for

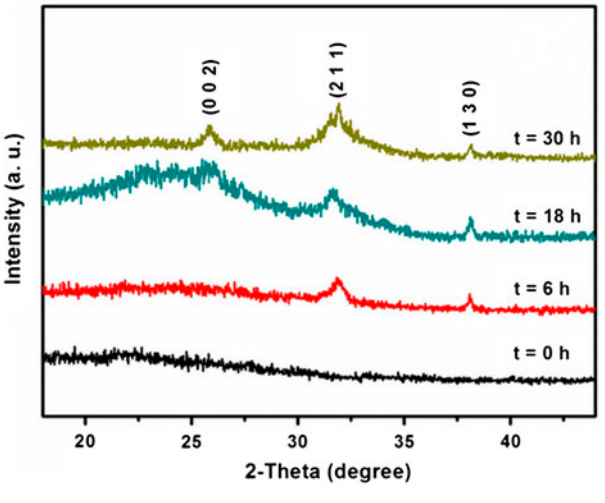

Figure 7. XRD patterns of BG/CNF composite nanofibers after soaking in 5SBF for different time.

30 h, the wide and dispersive peaks in XRD patterns indicated the formation of poorly crystallized or amorphous apatite after biological mineralization,[24] which was agreed well with FTIR analysis results.

Cell growth dynamics

Cell adhesion onto scaffolds was the first fundamental step in bone regeneration, which would greatly influence the morphology and capacity of cell proliferation and differentiation.[25] Therefore, the cell adhesion and subsequent growth were essentially important markers to determine whether materials could be used as scaffolds in bone

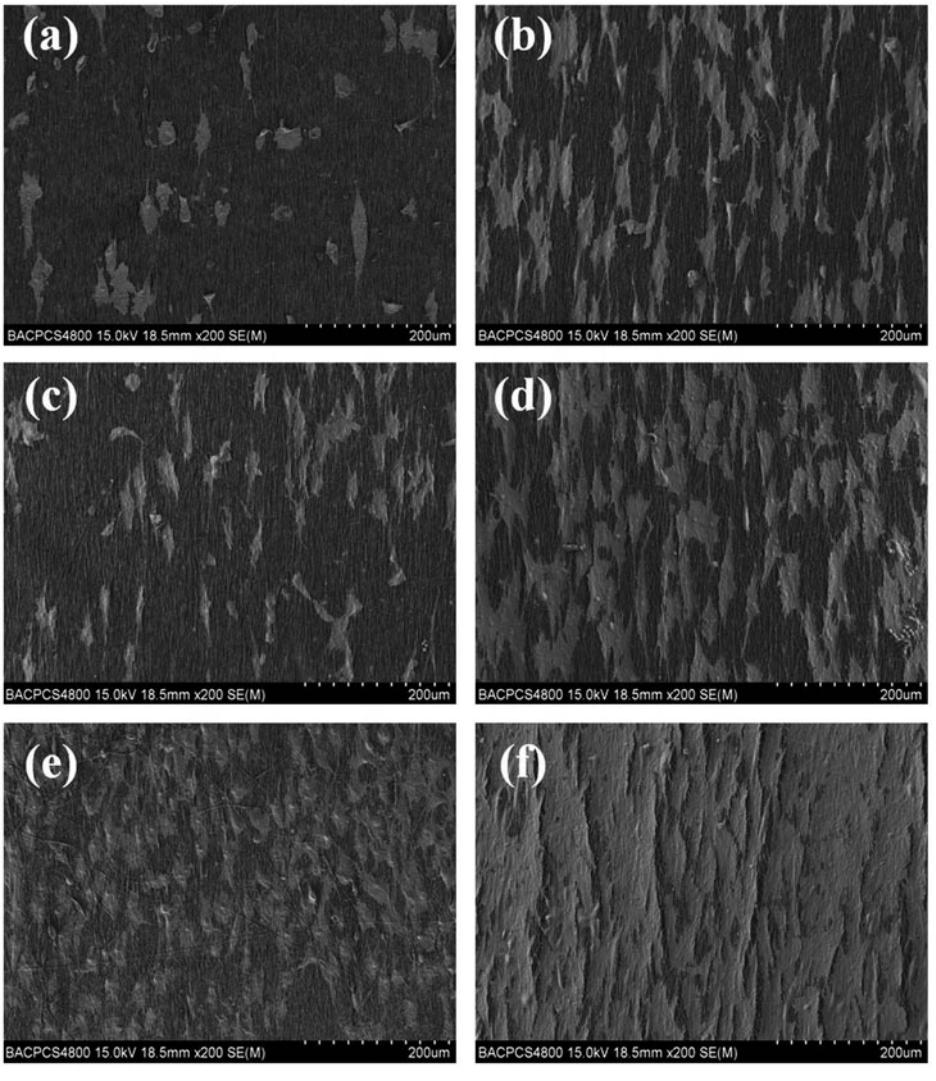

Figure 8. SEM images of BMSCs culture on PAN-based CNFs (a, c, e) and BG/CNF (b, d, f) composite nanofibers for 1 day (a, b), 3 days (c, d), and 5 days (e, f).

regeneration. Herein, BMSCs were cultured on the BG/CNF composite nanofibers and pure PAN-based CNFs to explore the cell growth dynamics, and the SEM images for 1, 3, and 5 days culture are shown in Figure 8. SEM observation found that BMSCs adhered and grew well on both nanofibrous membranes, and the cell proliferation increased with the increase of seeding time. Meanwhile, the BG/CNF composite nanofibers showed better BMSCs adhesion and proliferation than those on pure PAN-based CNFs. Especially after 5 days seeding, cells were confluent and appeared as a dense network throughout the BG/CNF composite nanofibers, which indicated a higher biocompatibility of BG/CNF composite nanofibers than pure PAN-based CNFs.

From CCK-8 assay, time-dependent BMSCs viability increase in all groups was observed in Figure 9. The BMSCs cultured on the BG/CNF composite nanofibers showed better proliferation performance than those cultured on PAN-based CNFs. The result was consistent with the aforementioned results in SEM observations, which may be ascribed to the more adhesion sites for BMSCs provided by the BG nanoparticles on the external surfaces of composite nanofibers.[26] In addition, the ions such as Na^{+} and Ca^{2+} released by degradation of BG provided more nutrition for the growth of bone tissue cell on the CNFs.[27]

As an important factor in determining bone differentiation, mineralization and a potent inducer of bone formation, the ALP activity secreted by the cells on both nanofibrous membranes was compared, as shown in Figure 10. For all groups, the ALP expression was up-regulated throughout the osteogenic induction culturing period. Obviously, the ALP level on day 7 was significantly higher on the BG/CNF composite nanofibers and still remained significantly higher expression level on day 14 than those on pure PAN-based CNFs, which suggested the osteogenic differentiation of BMSCs was up-regulated in response to the doping of BG in PAN-based CNFs. Similar results were obtained in several previous research about the osteoinductive effect of BG materials. Valimaki [28] indicated that BG microsphere induced a long-lasting production of bone matrix with concurrent upregulation of osteoclastic markers. The controlled release of biologically active Ca and Si ions from BGs was also reported to up-regulate and activate of seven families of genes in osteoprogenitor cells that give

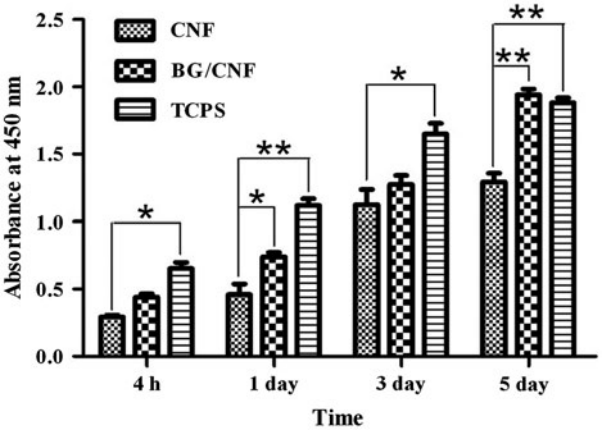

Figure 9. Cell proliferation analyzed by the absorbance measured at 450 nm for the indicated samples for 4 h, 1, 3, and 5 days. In the graphs (*) represents $p < 0.05$, and (**) $p < 0.01$.

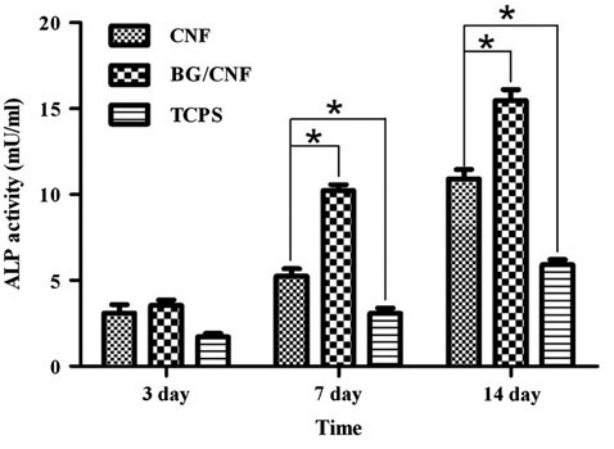

Figure 10. Quantification of ALP activity in culture supernatants of BMSCs after 3, 7, and 14 days cultured with osteogenic differentiation medium in the indicated groups. In the graphs (*) represents $p < 0.05$.

rise to rapid bone regeneration.[29] The mechanism of improved osteointegration of BG has been attributed to the formation of an apatite layer on its surface. The driving force for apatite formation is the release of ions such as Na+ and Ca2+ during degradation of BG when it is in contact with body fluid.[30,31] With the improved bioactivity by incorporating BG, the BG/CNF composite nanofibers were more favorable than pure PAN-based CNFs to be applied as scaffolds for bone tissue engineering. These positive results constitute the necessary prerequisites for further investigations into the potential of the BG materials to direct osteogenesis, leading to subsequent bone tissue regeneration.

Conclusions

BG/CNF composite nanofibers has been successfully fabricated by electrospinning from PAN/CN/TEP/TEOS solution and followed by *in situ* sintering. Microstructure and phase composition analysis indicated that the resulting materials were fine bioglass particles attached to the surface of the PAN-based CNFs. The biological mineralization evaluation identified the formation of the apatite-like layer consisting of crystallites of CHA. Cellular morphology, CCK-8 assay, and ALP activity assay suggested that BG/CNF composite nanofibers possessed favorable degradation and bioactivity, which may be one of promising biomaterials for facilitation of osteogenesis.

Funding

The authors would acknowledge financial support from National Basic Research Program of China [number 2012CB933900], the Key Technologies R&D Program of China [2012BAI07B00]; the National High Technology Research and Development Program of China [2011AA030100]; the Beijing municipal Science & Technology Commission Projects [number Z121100005212007]; the Key International S&T Cooperation Projects [number 2011DFA32190]; and the Science Foundation of Peking University School and Hospital of Stomatology [number YS020212].

References

[1] Kettunen J, Makela EA, Miettinen H, Nevalainen T, Heikkila M, Pohjonen T, Tormala P, Rokkanen T. Mechanical properties and strength retention of carbon fiber-reinforced liquid crystalline polymer (LCP/CF) composite: an experimental study on rabbits. Biomaterials. 1998;19:1219–1228.

[2] Peters JL, Miner LH, Michael AC, Sesack SR. Ultrastructure at carbon fiber microelectrode implantation sites after acute voltammetric measurements in the striatum of anesthetized rats. J. Neurosci. Methods. 2004;137:9–23.

[3] Aoki K, Usui Y, Narita N, Ogiwara N, Iashigaki N, Nakamura K, Kato H, Sano K, Ogiwara N, Kametani K, Kim C, Taruta S, Kim YA, Endo M, Saito N. A thin carbon-fiber web as a scaffold for bone-tissue regeneration. Small. 2009;5:1540–1546.

[4] Webster TJ, Waid MC, McKenzie JL, Price RL, Ejiofor JU. Nano-biotechnology: carbon nanofibres as improved neural and orthopaedic implants. Nanotechnology. 2004;15:48–54.

[5] McKnight TE, Ericson MN, Jones SW, Melechko AV, Simpson ML. Vertically aligned carbon nanofiber arrays: an electrical and genetic substrate for tissue scaffolding. Conf. Proc. IEEE Eng. Med. Biol. Soc. 2007;26:5381–5383.

[6] Elias KL, Price RL, Webster TJ. Enhanced functions of osteoblasts on nanometer diameter carbon fibers. Biomaterials. 2002;23:3279–3287.

[7] Kobayashi S, Kawai W. Development of carbon nanofiber reinforced hydroxyapatite with enhanced mechanical properties. Composites Part A. 2007;38:114–123.

[8] Zhang YZ, Venugopal J, Huang ZM, Lim CT, Ramakrishna S. Crosslinking of the electrospun gelatin nanofibers. Polymer. 2006;47:2911–2917.

[9] Kashyap S, Griep K, Nychka JA. Crystallization kinetics, mineralization and crack propagation in partially crystallized bioactive glass 45S5. Mater. Sci. Eng., C. 2011;31:762–769.

[10] Tomsia AP, Saiz E, Song J, CR. Biomimetic bonelike composites and novel bioactive glass coatings. Adv. Eng. Mater. 2005;7:999–1004.

[11] Hench LL. The role of ceramics in an age of biology. Bioceramics: Mater. Appl. IV. 2003;147:3–12.

[12] Hench LL. Genetic design of bioactive glass. J. Eur. Ceram. Soc. 2009;29:1257–1265.

[13] Gunawidjaja PN, Lo AYH, Izquierdo-Barba I, Garcia A, Arcos D, Stevensson B, Grins J, Vallet-Regi M, Eden M. Biomimetic apatite mineralization mechanisms of mesoporous bioactive glasses as probed by multinuclear P-31, Si-29, Na-23 and C-13 solid-state NMR. J. Phys. Chem. C. 2010;114:19345–19356.

[14] Labbaf S, Tsigkou O, Muller KH, Stevens MM, Porter AE, Jones JR. Spherical bioactive glass particles and their interaction with human mesenchymal stem cells *in vitro*. Biomaterials. 2011;32:1010–1018.

[15] Hench LL, Xynos ID, Polak JM. Bioactive glasses for *in situ* tissue regeneration. J. Biomater. Sci., Polym. Ed. 2004;15:543–562.

[16] Liu HY, Cai Q, Lian PF, Fang Z, Duan S, Ryu S, Yang XP, Deng XL. The biological properties of carbon nanofibers decorated with beta-tricalcium phosphate nanoparticles. Carbon. 2010;48:2266–2272.

[17] Liu HY, Cai Q, Lian PF, Fang Z, Duan S, Yang XP, Deng XL, Ryu S. Beta-tricalcium phosphate nanoparticles adhered carbon nanofibrous membrane for human osteoblasts cell culture. Mater. Lett. 2010;64:725–728.

[18] Xia W, Chang J. Preparation, *in vitro* bioactivity and drug release property of well-ordered mesoporous 58S bioactive glass. J. Non-Cryst. Solids. 2008;354:1338–1341.

[19] Barrere F, van Blitterswijk CA, de Groot K, Layrolle P. Nucleation of biomimetic Ca-P coatings on Ti6Al4V from a SBF × 5 solution: influence of magnesium. Biomaterials. 2002;23:2211–2220.

[20] Bowker M. Surface science – the going rate for catalysts. Nat. Mater. 2002;1:205–206.

[21] Dunham MG, Edie DD. Model of stabilization for PAN-based carbon-fiber precursor bundles. Carbon. 1992;30:435–450.

[22] Pacault A, Trinquecoste M. Carbonization kinetics of carbon-fiber precursors. Carbon. 1980;18:61–62.

[23] Ostomel TA, Shi QH, Tsung CK, Liang HJ, Stucky GD. Spherical bioactive glass with enhanced rates of hydroxyapatite deposition and hemostatic activity. Small. 2006;2:1261–1265.

[24] Vallet-Regi M, Romero AM, Ragel CV, LeGeros RZ. XRD, SEM-EDS, and FTIR Studies of *in vitro* growth of an apatite-like layer on sol-gel glasses. J. Biomed. Mater. Res. 1999;44:416–421.
[25] Kotaki MZ, Kotaki M, Yong T, He W, Ramakrishna S. Surface engineering of electrospun polyethylene terephthalate (PET) nanofibers towards development of a new material for blood vessel engineering. Biomaterials. 2005;26:2527–2536.
[26] Deng XL, Sui G, Zhao ML, Chen GQ, Yang XP. Poly(L-lactic) /hydroxyapatite hybrid nanofiberous scaffolds prepared by electrospinning. J. Biomater. Sci., Polym. Ed. 2007;8:117–130.
[27] Zanello LP, Zhao B, Hu H, Haddon RC. Bone cell proliferation on carbon nanotubes. Nano Lett. 2006;6:562–567.
[28] Valimaki VV, Yrjans JJ, Vuorio EL, Aro HT. Molecular biological evaluation of bioactive glass microspheres and adjunct bone morphogenetic protein 2 gene transfer in the enhancement of new bone formation. Tissue Eng. 2005;11:387–394.
[29] Hench Larry L. Genetic design of bioactive glass. J. Eur. Ceram. Soc. 2009;29:1257–1265.
[30] Grenspan DC, Zhong JP, Chen ZF, LaTorre GP. The evaluation of degradability of melt and sol-gel derived bioglass *in vitro*. Bioceramics. 1997;10:391–394.
[31] Rahaman MN, Day DE, Bal BS, Fu Q, Jung SB, Bonewald LF, Tomsia AP. Bioactive glass in tissue engineering. Acta Biomater. 2011;7:2355–2373.